

# Journal of Visualized Experiments

## Fabrication and characterization of optical tissue phantoms containing macrostructure --Manuscript Draft--

<b>Article Type:</b>	Methods Article - JoVE Produced Video
<b>Manuscript Number:</b>	JoVE57031R1
<b>Full Title:</b>	Fabrication and characterization of optical tissue phantoms containing macrostructure
<b>Keywords:</b>	Tissue simulating phantoms; optical imaging; calibration standard; quality assurance; computer model validation; 3D printing
<b>Corresponding Author:</b>	Kristen C. Maitland, Ph.D. Texas A&M University College Station College Station, TX UNITED STATES
<b>Corresponding Author's Institution:</b>	Texas A&M University College Station
<b>Corresponding Author E-Mail:</b>	kmaitland@tamu.edu
<b>First Author:</b>	Madeleine Durkee
<b>Other Authors:</b>	Madeleine Durkee
	Landon Nash
	Fatemeh Nooshabadi
	Jeffrey Cirillo
	Duncan Maitland
<b>Author Comments:</b>	
<b>Additional Information:</b>	
<b>Question</b>	<b>Response</b>
If this article needs to be "in-press" by a certain date, please indicate the date below and explain in your cover letter.	

**TITLE**

Fabrication and characterization of optical tissue phantoms containing macrostructure

**AUTHORS & AFFILIATIONS**

Madeleine S. Durkee<sup>1</sup>, Landon D. Nash<sup>1</sup>, Fatemeh Nooshabadi<sup>1</sup>, Jeffrey D. Cirillo<sup>2</sup>, Duncan J. Maitland<sup>1</sup>, Kristen C. Maitland<sup>1</sup>

<sup>1</sup>Department of Biomedical Engineering, Texas A&M University, College Station, TX, USA

<sup>2</sup>Department of Molecular Pathogenesis and Immunology, Texas A&M College of Medicine, Bryan, TX, USA

**CORRESPONDING AUTHOR:**

Kristen C. Maitland

Email Address: [kmaitland@tamu.edu](mailto:kmaitland@tamu.edu)

Tel: (979) 845-1864

**EMAIL ADDRESSES OF CO-AUTHORS:**

Madeleine S. Durkee [madeleine.simonne@gmail.com](mailto:madeleine.simonne@gmail.com)

Landon D. Nash [nashlandon@gmail.com](mailto:nashlandon@gmail.com)

Fatemeh Nooshabadi [fatemeh.n@gmail.com](mailto:fatemeh.n@gmail.com)

Jeffrey D. Cirillo [jdcirillo@gmail.com](mailto:jdcirillo@gmail.com)

Duncan J. Maitland [djmaitland@tamu.edu](mailto:djmaitland@tamu.edu)

**KEYWORDS**

Tissue simulating phantoms, optical imaging, calibration standard, quality assurance, computer model validation, 3D printing

**SHORT ABSTRACT**

Optical tissue phantoms are essential tools for calibration and characterization of optical imaging systems and validation of theoretical models. This article details a method for phantom fabrication that includes replication of tissue optical properties and three-dimensional tissue structure.

**LONG ABSTRACT**

The rapid development of new optical imaging techniques is dependent on the availability of low-cost, customizable, and easily reproducible standards. By replicating the imaging environment, costly animal experiments to validate a technique may be circumvented. Predicting and optimizing the performance of *in vivo* and *ex vivo* imaging techniques requires testing on samples that are optically similar to tissues of interest. Tissue-mimicking optical phantoms provide a standard for evaluation, characterization, or calibration of an optical system. Homogenous polymer optical tissue phantoms are widely used to mimic the optical properties of a specific tissue type within a narrow spectral range. Layered tissues, such as the epidermis and dermis, can be mimicked by simply stacking these homogenous slab phantoms. However, many *in vivo* imaging techniques are applied to more spatially complex tissue where three dimensional structures, such as blood vessels, airways, or tissue defects, can affect the performance of the

imaging system.

This protocol describes the fabrication of a tissue-mimicking phantom that incorporates three-dimensional structural complexity using material with optical properties of tissue. Look-up tables provide India ink and titanium dioxide recipes for optical absorption and scattering targets. Methods to characterize and tune the material optical properties are described. The phantom fabrication detailed in this article has an internal branching mock airway void; however, the technique can be broadly applied to other tissue or organ structures.

## INTRODUCTION

Tissue phantoms are used widely for system characterization and calibration of optical imaging and spectroscopy instruments, including multimodality systems incorporating ultrasound or nuclear modalities<sup>1-4</sup>. Phantoms provide a controlled optical environment for system characterization and quality control of multiple biological imaging techniques. Tissue-mimicking phantoms are useful tools in predicting system performance and optimizing system design for the physiological task at hand; for example, to predict the probing depth of spectroscopic probes for assessing tumor margins<sup>5</sup>. Optical properties and structural design of the phantoms can be tuned to mimic the specific physiological environment in which the instrument will be used, therefore allowing for both feasibility studies and verification of system performance<sup>3,6,7</sup>. Verification of imaging system performance with realistic optical phantoms prior to entering pre-clinical or clinical trials reduces the risk of malfunction or acquisition of unusable data during *in vivo* studies. The reproducibility and stability of optical phantoms make them customizable calibration standards for optical techniques to monitor intra- and inter-instrument variability, particularly in multicenter clinical trials with different instruments, operators, and environmental conditions<sup>8,9</sup>.

Tissue-mimicking phantoms also serve as tunable and reproducible physical models for validation of theoretical optical models. Simulations aid in the design and optimization of *in vivo* optical instruments, while reducing the need for animal experiments<sup>10,11</sup>. The development and validation of optical simulations to accurately represent the *in vivo* environment can be encumbered by the complexity of the tissue structure, the biochemical content, and the location of the target or tissue within the body. Variability between subjects makes validation of theoretical models challenging using animal or human measurements. Polymer optical tissue phantoms allow for validation of theoretical models by supplying a known and reproducible optical environment in which to study photon migration<sup>12-15</sup>.

For the purpose of system calibration, solid optical phantoms may consist of a single homogeneous slab of cured polymer with the optical scattering, absorption, or fluorescence tuned for the wavelengths of interest. Layered polymer phantoms are frequently used to mimic the depth variance of the tissue optical properties in epithelial tissue models<sup>16,17</sup>. These phantom structures are sufficient for epithelial imaging and modeling, because the tissue structure is fairly homogeneous through each layer. However, larger scale and more complex structures affect radiative transport in other organs. Methods to create more complex phantoms have been developed to simulate the optical environment of subcutaneous blood vessels<sup>18,19</sup> and even

whole organs, such as the bladder<sup>20</sup>. Modeling light transport in the lungs provides a unique problem due to the branching structure of the air-tissue interface; a solid phantom would not likely replicate radiative transport in the organ accurately<sup>21</sup>. To describe a method for incorporating complex structure into an optical phantom, we describe a method to create an internal, reproducible fractal tree void that represents the three-dimensional (3D) macroscopic structure of the airway (**Figure 1**).

In the past few decades, 3D printing has become a predominant method for rapid prototyping of medical devices and models<sup>22</sup>, and optical tissue phantoms are no exception. 3D printing has been used as an additive manufacturing tool for fabricating optical phantoms with channels<sup>23</sup>, blood vessel networks<sup>24</sup>, and whole-body small animal models<sup>25</sup>. These methods use one or two printing materials with unique optical properties. Methods have also been developed to tune the optical properties of the printing material to mimic general, turbid biological tissue<sup>25,26</sup>. However, the range of achievable optical properties are limited by the printing material, usually a polymer such as acrylonitrile butadiene styrene (ABS)<sup>26</sup>, so this method is not suitable for all biological tissues. Polydimethylsiloxane (PDMS) is an optically clear polymer that can be readily mixed with scattering and absorbing particles with a higher level of tunability<sup>27,28</sup>. PDMS has also been used to mold phantoms with aneurysm models for deployment of embolic devices<sup>29,30</sup>. These phantoms also utilize a dissolvable 3D printed part, but remain optically clear for visualizing device deployment. Here, we combine this method with tunability of the optical properties of PDMS with scattering and absorbing particles to fabricate a preliminary model of the tissue and airways of the murine lung.

While the phantom presented here is specific to the lungs, the process can be applied to a variety of other organs. 3D printing of the internal structure of the phantom allows the design to be customizable for any purpose and printable scale, whether it be a blood or lymph vessel network, bone marrow, or even the four chambered structure of the heart<sup>31</sup>. Because we are interested in optical imaging and modeling of the lung<sup>32-34</sup>, we have opted to use a four-generation fractal tree as the internal structure to replicate within the polymer phantom. This structure was designed to approximate the branching structure of the airway and have break-away support material for the 3D printing process. A more anatomically correct airway could be printed if break-away support material is not necessary. Although this particular model represents an airway, the internal structure of the phantom does not have to remain a material void. Once the surrounding polymer is cured and the 3D printed part is dissolved, the internal structure can be used as a flow pathway or as a secondary mold for a material with its own unique absorption and scattering characteristics. For example, if the internal structure from this protocol was designed as a digital bone rather than an airway, the bone structure could be 3D printed, molded with PDMS with optical properties of the finger, and then dissolved out of the phantom. The void could then be filled with a PDMS mixture with different optical properties. Additionally, each mold is not limited to a single dissolvable part. A phantom of the finger could be created to include bone, veins, arteries, and a general soft tissue layer, each with its own unique optical properties.

## **PROTOCOL**

### **1. Selection and Verification of Matrix Material Properties**

1.1. Before starting the phantom fabrication process (**Figure 1**), find the absorption and reduced scattering coefficients for the biological tissue of interest at the imaging wavelength(s). Preliminary estimates may be found in the references<sup>35,36</sup>. However, validation of the optical coefficients might be necessary.

1.2. Using the look-up tables for absorption coefficient,  $\mu_a$ , and reduced scattering coefficient,  $\mu_s'$ , at 488, 535, 632, and 775 nm wavelengths (**Tables 1–4** and **Figures 2–3**), select the concentrations of India ink and titanium dioxide ( $\text{TiO}_2$ ) that approximate the desired optical properties. These recipes are specific to phantoms fabricated with PDMS. As these tables provide experimental data at discrete wavelengths, optimization of the recipe may be required for the specific application.

1.3. Fabricate a polydimethylsiloxane (PDMS) slab of the selected recipe for confirmation of optical properties.

1.3.1. Using a 10:1 ratio in weight of PDMS resin to curing agent, pour ingredients into the mixing cup in the following order: PDMS resin,  $\text{TiO}_2$ , India ink, PDMS curing agent.

Note: Here, we test two recipes: 1) 2 mg  $\text{TiO}_2$  + 3.5  $\mu\text{L}$  India ink per g PDMS and 2) 1 mg  $\text{TiO}_2$  + 10  $\mu\text{L}$  India ink per g PDMS. For each recipe, 4.5 g PDMS resin and 0.45 g PDMS curing agent are used with the corresponding amounts of optical particles.

1.3.2. Mix in a speed mixer (see **Table of Materials**) for 60 s. If  $\text{TiO}_2$  particles stick to the mixing cup (probable with high concentrations of  $\text{TiO}_2$ ), mix by hand to remove the particles from the base of the cup, and mix in the mixer for another 30 s.

1.3.3. Pour the mixture into wells or Petri dishes to make thin (0.1–1 mm) slabs of the mixture.

1.3.4. Degas the slabs for 10 min by placing them in an air-tight negative pressure chamber, then place in a pre-heated oven at 80 °C for 30–60 min. Remove from oven and let cool.

1.3.5. Remove the cooled polymer slab from its container. Trim off the edges to leave a flat, uniform slab. Measure the thickness of the slab using calipers.

1.4. Measure transmittance (T) and reflectance (R) of slab(s) using an integrating sphere. Additional details and instructions can be found in the Inverse-Adding Doubling (IAD) manual<sup>37</sup>.

1.4.1. Turn on the light source and spectrometer of the integrating sphere setup. Check the alignment of the system to ensure a small, collimated beam is centered on the entry and exit ports of the integrating sphere.

1.4.2. Calibrate the integrating sphere system.

1.4.2.1. Turn off the source, cap the exit port of the integrating sphere, and record three dark spectra.

1.4.2.2. Turn the source back on to obtain the transmission reference with the exit port capped and the entrance port empty. Record three spectra.

1.4.2.3. Obtain reflectance reference measurements using reflectance standard(s). Place each standard at the exit port of the sphere. Record three spectra for each reflectance standard.

1.4.3. Measure the transmittance of the slab. With the cap on the exit port, place the slab on the entry port of the integrating sphere for the transmission measurement. Record three spectra.

1.4.4. Measure the reflectance of the slab. Remove the exit port cap and place the slab on the exit port for the reflectance measurement. Record three spectra.

1.5. Determine optical properties using IAD software. A full tutorial on the software can be found in the IAD manual with the software download<sup>37,38</sup>.

1.5.1. Average the three spectra acquired for each measurement.

1.5.2. Using the equations in the IAD manual<sup>37</sup>, convert these measurements to R and T values. If necessary, condense the files by reducing the sampling rate along the spectrum.

1.5.3. Prepare the input .rxt file (**Supplemental Material 1**) for IAD with the wavelengths, reflectance, transmittance, and sample thickness as described in the IAD manual<sup>37</sup>. Using the command prompt (Windows OS) or terminal (Mac OS), navigate to the correct path. Type "iad 'input file name'" to run IAD. The software will produce an output text file with the estimated optical properties.

1.6. If the optical properties are not within an acceptable range (~15%) of the desired values, modify the recipe accordingly and repeat steps 1.3-1.5.

## 2. Preparation of Dissolvable 3D Printed Internal Structure

2.1. Design internal structure using computer aided design (CAD) software. Convert structure solid model to a stereolithography file for fabrication on a 3D printer. If available, a segmented CT scan can also be converted into a stereolithography file rather than drawing a solid model of the internal structure.

Note: The CAD file for the fractal tree structure used here is provided in **Supplemental Material 2**. The printer used in this paper is an extruding printer, so the part was designed to have break-away support material.

2.2. Select a dissolvable material for printing, such as poly-vinyl alcohol (PVA) or high-impact

polystyrene (HIPS) (see **Table of Materials**). Print the solid model in this dissolvable material.

2.3. When printed parts are sufficiently cooled, break, dissolve, or machine the support material off of the printed part. File or sand off any large imperfections.

2.4. Vapor polish the printed part to reduce surface roughness.

2.4.1. With the printed part secured in a vice, drill a through hole with clearance for a thin steel or nitinol wire in the base of the printed part.

2.4.2. Thread a stainless steel or nitinol wire through the hole. Bend ends of wire and hook together. This will allow for the part to be fully immersed in acetone vapor within the beaker. Set wire and part aside.

2.4.3. Fill a large beaker roughly 10% full of acetone. Place beaker on a hot plate while heating to 100 °C. CAUTION: Perform this step in a fume hood to prevent inhalation of acetone vapor.

2.4.4. When acetone vapor condensation reaches about halfway up the wall of the beaker, hang the looped wire with the mock airway on a second wire and suspend in acetone vapor for 15–30 s. Ensure printed parts do not touch the beaker walls or each other (if vapor polishing multiple parts at once).

2.4.5. Remove printed part and suspend over empty beaker or container. Let part dry for at least 4 h.

2.5. Verify the dimensions of the internal structure are within tolerance to the CAD design, as needed. Depending on accuracy requirements, calipers or a 3D laser scanner can be used to measure the structure.

### **3. Construction of Heat Resistant Mold**

Note: Prepare a leak-proof, heat-resistant mold to form the PDMS phantom. Select a mold geometry to best fit the final phantom design. Here, a reusable rectangular mold is described.

3.1. Design a solid model base of the mold to 3D print. This mold is designed for a phantom with a base of 1.17 cm x 1.79 cm. The base of the mold has a 1 mm thick and 5 mm deep recess with inner dimensions matching the base of the phantom. This allows the mold to sidings to be removed and the mold to be disassembled and re-used.

3.2. Print a base for the mold with an inset of sufficient width to secure the sidings of the mold.

3.3. Place sidings in the recesses of the mold base. Here, 1 mm thick polycarbonate sheets are used as mold sidings.

3.4. Using heat resistant tape, seal the edges of the mold. It is imperative that all corners and edges are sufficiently sealed with no bubbles in the tape to prevent any leakage during the molding process.

3.5. Place a polycarbonate base plate inside the mold prepared in step 3.4. This base plate is the same 1 mm thick polycarbonate sheet as the mold siding and gives the phantom base a smooth surface without the roughness of the 3D printed surface of the mold base. Glue the fully-dried vapor polished part to the base plate. Allow sufficient time for glue to dry.

#### 4. Fabrication of Polymer Phantom

Note: Use the verified recipe for the bulk matrix material determined in step 1 for the specific application. The protocol here provides the steps for a healthy murine lung tissue phantom at 535 nm with  $\mu_s'$  of  $40 \text{ cm}^{-1}$  and  $\mu_a$  of  $2 \text{ cm}^{-1}$ . It may be useful to fabricate a second phantom with no optical particles to use as a reference in the fabrication process.

4.1. Pour 9.1 g of PDMS resin into a plastic mixing cup. Add 20 mg of rutile  $\text{TiO}_2$ , followed by 35  $\mu\text{l}$  of India ink. Finally add 0.91 g of curing agent to the top of the mixture. Follow the mixing protocol in step 1.3.2.

4.2. Pour final polymer mixture into the heat-resistant mold.

4.3. Pour a small amount of the mixture into a separate container to create a polymer slab for confirmation of material optical properties. Ensure enough polymer is poured to have a slab of at least 100  $\mu\text{m}$  thickness.

4.4. Place both the mock airway mold and the separate slab into a bell jar for degassing. Begin vacuum process. If the polymer in the mock airway mold starts to rise, let the air back into the bell jar to burst the surface bubbles, then begin to pull air again. Repeat this process until the polymer does not rise significantly. This will take between 5-10 min depending on how much air was trapped during step 4.2. Once the PDMS no longer rises, continue to degas for another 15 min.

4.5. After degassing, slowly let the air back into the chamber. Remove both the mock airway phantom and the polymer slab and place in level oven at  $80^\circ\text{C}$  for 2 h.

4.6. Remove the phantom and slab from the oven and let cool for 20 min. Disassemble the polymer mold with a scalpel without cutting the cured polymer. Snap the base plate off of the mock-airway base.

4.7. Place phantom in a heated ( $60^\circ\text{C}$ )  $\sim 0.5 \text{ M}$  sodium hydroxide ( $\text{NaOH}$ ) base bath until the internal part is fully dissolved. An optically clear reference phantom may help to determine the dissolving time for the internal component. Once internal structure is dissolved, take phantom out of the bath and let fully dry ( $\sim 24 \text{ h}$ ) before taking any optical measurements.



## 5. Verification of Phantom Fabrication

5.1. Verify phantom geometry using high resolution magnetic resonance imaging (MRI) or micro-computed tomography (CT) imaging, if desired. These methods provide a 3D verification of internal structures within turbid material with axial resolutions of  $<400\text{ }\mu\text{m}$ <sup>39,40</sup>. Alternatively, an optically clear reference phantom can be optically imaged for verification that the printed part is fully dissolved and the remaining void is the correct geometry.

Note: We have verified the internal geometry of an optically opaque phantom (2 mg  $\text{TiO}_2$  + 3.5  $\mu\text{l}$  India ink) with micro-CT on a North Star Imaging (NSI) X50. The phantom was imaged with 20  $\mu\text{m}$  resolution in all dimensions (**Supplemental Materials 3, 4**).

5.2. Verify optical properties of the phantom using the polymer slab and the integrating sphere (described in steps 1.5-1.6).

## REPRESENTATIVE RESULTS

To demonstrate the phantom fabrication technique, mouse lung tissue phantoms were fabricated to simulate measured optical properties of excised healthy and inflamed murine lung tissue at 535 nm (**Table 5**). This wavelength of interest is the excitation wavelength for tdTomato fluorescent protein used in recombinant reporter strains of mycobacteria in previous studies<sup>33</sup>. Optical measurements of mouse lung tissue were obtained with the same methods described in steps 1.4–1.5. Use of animals was approved by the Institutional Animal Care and Use Committee (IACUC) at Texas A&M University. A suitable ratio of  $\text{TiO}_2$  to India ink was found for both healthy and inflamed murine lung tissue for 535 nm wavelength light (**Table 5**).

Recipes for materials with different optical properties are shown in **Tables 1-4** and graphically in **Figures 2–3**. The dependence of absorption and scattering on particle concentration are summarized in **Figure 4**. Trends in absorption coefficient and reduced scattering coefficient for phantoms with a constant concentration of  $\text{TiO}_2$  (scattering particle) (**Figure 4A, 4B**) and a constant concentration of India ink (absorbing particle) (**Figure 4C, 4D**) demonstrate the relation of optical properties to both particles. To ensure reproducibility of these optical properties, proper mixing technique must be used. Settling and ribboning of  $\text{TiO}_2$  particles will cause a shift in the scattering coefficient of the cured phantom (**Figure 5**). India ink staining the mixing container will also reduce the absorption coefficient.

The lung phantoms were designed using a fractal tree structure for the internal void (**Figure 1C**). The 3D printed structure must be vapor polished to create a smooth internal surface inside the phantom (**Figure 1E**). **Figure 6** shows a comparison of light scattering from a phantom that was not degassed or vapor polished (**Figure 6A, 6C**), and a phantom that had a vapor polished internal part and was degassed (**Figure 6B, 6D**). The phantoms were imaged using illumination from an external white light source (**Figure 6A, 6B**) and with an internal microendoscope source at 535 nm (**Figure 6C, 6D**). Vapor polishing and degassing minimize the presence of irreproducible scatterers, including surface roughness (**Figure 6C**, inset 2) and bubbles (**Figure 6C**, inset 1).

Degassing is particularly important, because air bubble location is random and unpredictable. Furthermore, air bubbles are obscured once TiO<sub>2</sub> particles are incorporated (not shown in **Figure 6**), making the phantom optically opaque. Therefore, unseen bubbles may undermine the phantom material's representation of tissue optical properties.

The vapor-polished 3D printed part was measured with calipers at the base and at the distal branches, and dimensions are compared to the 3D solid model in **Table 6**. Following fabrication of the polymer phantom, the phantom was imaged using a micro-CT imaging system (**Supplemental Material 3**). Using the 3D dataset, dimensions of the internal void at the base and distal branches were measured for comparison (**Table 6**). The vapor polished tree is slightly smaller at the base because the smoothing of the surface by the acetone vapor causes the surface of the plastic to flow. With the 3D printed part suspended by the base, the surface flows towards the distal branches, causing a small change in dimension of the part. There is a trade-off between surface smoothness and maintaining part size. A longer vapor polish will result in a smoother surface, but will cause more material to flow, resulting in altered dimensions.

Phantoms were imaged in an *in vivo* imaging system with an access port for insertion of a microendoscope fiber bundle (**Figure 7**). The microendoscope was placed into the void within the phantoms from which the printed part had been dissolved. The microendoscope was used for internal illumination at 535 nm and the IVIS illumination pathway was blocked. The placement of the microendoscope is indicated in **Figure 7A**. The IVIS was used for external collection of signal. Phantoms imaged had the same internal structure as those imaged in **Figure 3**. With identical internal structures and external dimensions, the difference in optical properties between healthy lung tissue (**Figure 7A**) and infected lung tissue (**Figure 7B**) is apparent in the surface irradiance of the phantoms. As these phantoms maintain an appropriate response to a change in optical properties, this method for phantom fabrication can be applied for phantoms used in internal illumination studies.

## FIGURE AND TABLE LEGENDS

**Figure 1. Flow diagram of fabrication of optical tissue phantom.** (A) Determine optimal recipe for target optical properties of tissue of interest. (B) Verify recipe. (C) Design internal structure. (D) Print internal structure using dissolvable material. (E) Vapor polish printed part to smooth surface. (F) Mix polymer and optical particles, and pour into heat-resistant mold. (G) Degas and cure polydimethylsiloxane (PDMS). (H) Dissolve printed part to create internal void. (I) Verify phantom geometry and optical properties.

**Figure 2. Trends in absorption coefficient for India ink and TiO<sub>2</sub> concentration.** Absorption coefficients are shown for a range of India ink and titanium dioxide concentrations at 488 nm (A), 535 nm (B), 630 nm (C), and 775 nm (D). Absorption is low for low concentrations for both particles, and generally increases with concentrations of each particles. A plateau is reached between 5-7.5  $\mu$ L India ink per mL PDMS. The rate of increase depends on the concentration of the other particle and the wavelength.

**Figure 3. Trends in reduced scattering coefficient for India ink and TiO<sub>2</sub> concentration.** Reduced scattering coefficients are shown for a range of India ink and titanium dioxide concentrations at 488 nm (A), 535 nm (B), 630 nm (C), and 775 nm (D). The reduced scattering coefficient is low for low concentrations for both particles, and generally increases with concentrations of each. Like absorption, the rate of increase depends on the concentration of the other particle and the wavelength.

**Figure 4. Interdependency of optical properties on India ink and TiO<sub>2</sub> concentration.** Absorption coefficients and reduced scattering coefficients are shown for recipes with a constant TiO<sub>2</sub> concentration of 1 mg/mL PDMS (A, B) and constant India ink concentration of 5 µL/mL PDMS (C,D). Panel (B) shows that scattering coefficient will change with a constant TiO<sub>2</sub> concentration when India ink concentration is varied, and panel (C) shows that absorption coefficient will change for a constant India ink concentration when TiO<sub>2</sub> is varied.

**Figure 5. Mixing effects on optical scattering.** Improper mixing of the uncured polymer and optical particles can result in a shift in the optical properties. The poorly mixed phantom represented in this figure showed settling of TiO<sub>2</sub> particles prior to curing.

**Figure 6. Representative airway phantoms with low scattering coefficient material to illustrate successful and suboptimal fabrication.** Vapor polishing and degassing are integral steps in producing a phantom that has minimal uncharacterized scattering elements. A-B) White light images of phantoms without vapor polishing and degassing (A) and with vapor polishing and degassing (B). C-D) Phantoms from A-B are illuminated with 535 nm light. Insets from (C) are shown to depict scattering effects of 1) air bubbles and 2) a rough 3D printed surface. E) Rendering of an optical simulation based on the computer aided design (CAD) model used for the phantom fabrication.

**Figure 7. Imaging of phantoms with internal illumination.** A computer simulation of the phantom (A) demonstrates the orientation of the internal geometry and source placement (yellow star) for the phantom images in panels (C) and (D). A segmented micro-CT scan of the healthy lung tissue phantom (B) confirms the internal structure is present in the optically opaque phantom. The mock airway is used as a pathway for the endoscope for internal illumination of the optical phantoms at a wavelength of 535 nm. The two phantoms imaged with internal illumination are identical in external shape and internal structure, with material optical properties optimized for healthy (C) and inflamed (D) lung tissue. All images and renderings are on the same scale. Scale bar in panel (C) is 1 cm.

**Table 1. Look-up table for 488 nm.**

**Table 2. Look-up table for 535 nm.**

**Table 3. Look-up table for 632 nm.**

**Table 4. Look-up table for 775 nm.**

**Table 5. Measured optical properties of phantom recipes correspond to the measured optical properties of healthy and inflamed mouse lung tissue at 535 nm.**

**Table 6. Verification of the internal structure of the phantom.**

**Supplemental Material 1. Example IAD input file.**

**Supplemental Material 2. Fractal tree airway solid model.**

**Supplemental Material 3. Micro-CT fly-thru of phantom modeling healthy mouse lung tissue.**

**Supplemental Material 4. Video of rotating segmented micro-CT scan.**

## **DISCUSSION**

We have demonstrated a method for creating optical phantoms to represent a murine lung with an internal branching structure to simulate the internal air-tissue interface. The optical properties of murine lung tissue are achieved by incorporating unique concentrations of optically scattering and absorbing particles distributed homogenously within the bulk matrix polymer. These optical properties can be tuned to mimic the physiological values within different spectral ranges of tissues in different states (i.e. healthy versus diseased tissue). The optical properties are dependent on the wavelength of interest, the base material, and the concentrations of the particles within the phantom. However, with multiple particles, the relationship between scattering and absorption is not always intuitive<sup>41</sup>. The rate of increase of absorption is dependent on the concentration of the scattering particle as well as the absorbing particle, and likewise for the rate of increase of the reduced scattering coefficient. (**Figures 2–4**). PDMS phantoms have also been shown to maintain their optical properties for up to 1 year<sup>27,28</sup>. We have measured a 3-week stability of optical properties within the error of our integrating sphere measurements (< 15%). Storage of these phantoms and standards in a light-tight container can help preserve their optical properties for longer periods of time.

Vapor polishing the dissolvable printed part allows for a reproducible smooth surface on the internal air interface of the phantom (**Figure 6**). For the fractal geometry shown here, polishing the internal structure yielded a decrease in average surface roughness of molded PDMS from 37.4  $\mu\text{m}$  to 7.2  $\mu\text{m}$ . This is extremely important if the phantom is used for validation of an optical simulation because a rough surface is much more difficult to accurately simulate than a smooth, uniform surface (**Figure 6E**). Degassing is also very important due to the fact that bubbles within the PDMS phantom act as optical scatterers (**Figure 6C**, inset 1). Bubble location is not predictable to replicate in a simulation, and could skew results if the phantom is used as a calibration standard.

After verification with micro-CT, a small amount of residual material was found within the airway void (**Supplemental Material 3**). Additionally, a segmentation of this same CT scan reveals a small

air bubble next to the branching structure (**Supplemental Material 4**). During fabrication, optically clear phantoms yielded a full dissolution of the material of the internal structure and no air bubbles within the polymer matrix. Verification with micro-CT showed that the optically opaque phantoms may contain small flaws, not otherwise visible.

Properly mixing the optical particles with the uncured polymer is imperative to achieve reproducible and predictable optical absorption and scattering. A shift in the reduced scattering coefficient caused by poor mixing is shown in **Figure 5**. Before pouring the polymer into the mold, ensure there is no evidence of TiO<sub>2</sub> particles settling or “ribboning” in the mixture and no evidence of India ink staining the mixing container. Adding the particles in the recommended order should minimize these problems.

The design of these phantoms is limited by the 3D printed part. The mock airway is designed so that the support material can be pried off, as it is not dissolvable. This can be overcome by moving to a more advanced printer that can either print materials with varying solubility, or a laser sintering printer, that does not need support material. It is also important to note that the lung is inherently a very porous organ because of the distal airways and the alveoli. While that is not represented in this phantom, the optical effects of similar structures have been observed using a Bragg-Nye bubble raft for optical coherence tomography<sup>21</sup>, air bubbles in olive oil<sup>42</sup>, and shaving cream or dish detergent for nuclear magnetic resonance imaging<sup>43</sup>. Creating polymer foams with reproducible characteristics may be able to reconcile this difference between the solid phantoms presented here and the lung microstructure<sup>44</sup>.

The shape of the final phantom can also be customized depending on the application. The rectangular phantom shown here was imaged with internal illumination and used for validation of a computational model of healthy and infected lungs (**Figure 7**). This design can be updated further to represent the cylindrical torso of the mouse by simply changing the design of the external polymer mold.

While we have detailed here the design of a murine lung and airway phantom, these methods can be modified to fit other organs or animals of interest. The internal structure can be converted to a flow pathway for vascular phantoms, or can be used as a cast for a complex internal structure with unique optical properties. The overall shape of the phantom can also be tuned to the application, animal, or organ of interest. 3D printing of both internal structures and polymer molds gives freedom to the design process of structured polymer optical phantoms. These are integral tools in simulation validation and calibration of *in vivo* optical imaging techniques, because they can more accurately represent the *in vivo* environment than homogeneous single or multi-layer phantoms.

## ACKNOWLEDGMENTS

This work was supported by the National Science Foundation CAREER award no. CBET-1254767 and National Institute of Allergy and Infectious Diseases grant no. R01 AI104960. We gratefully acknowledge Patrick Griffin and Dan Tran for their assistance with characterization measurements and the Texas A&M Cardiovascular Pathology Laboratory for micro-CT imaging.

## DISCLOSURES

The authors have nothing to disclose.

## REFERENCES

- 1 Curatolo, A., Kennedy, B. F., Sampson, D. D. Structured three-dimensional optical phantom for optical coherence tomography. *Opt Express*. **19** (20), 19480-19485, doi:10.1364/OE.19.019480, (2011).
- 2 Miranda, D. A., Cristiano, K. L., Gutiérrez, J. C. Breast phantom for mammary tissue characterization by near infrared spectroscopy. *J Phys Conf Ser*. **466** (1), 012018 (2013).
- 3 Solomon, M. *et al.* Multimodal Fluorescence-Mediated Tomography and SPECT/CT for Small-Animal Imaging. *J Nucl Med*. **54** (4), 639-646 (2013).
- 4 Wagnières, G. *et al.* An optical phantom with tissue-like properties in the visible for use in PDT and fluorescence spectroscopy. *Phys Med Biol*. **42** (7), 1415-1426 (1997).
- 5 Rajaram, N., Reesor, A. F., Mulvey, C. S., Frees, A. E., Ramanujam, N. Non-Invasive, Simultaneous Quantification of Vascular Oxygenation and Glucose Uptake in Tissue. *PLoS ONE*. **10** (1), e0117132, doi:10.1371/journal.pone.0117132, (2015).
- 6 Niedre, M. J., Turner, G. M., Ntziachristos, V. Time-resolved imaging of optical coefficients through murine chest cavities. *J Biomed Opt*. **11** (6), 064017, doi:10.1117/1.2400702, (2006).
- 7 Schmidt, F. E. W. *et al.* Multiple-slice imaging of a tissue-equivalent phantom by use of time-resolved optical tomography. *Appl Opt*. **39** (19), 3380-3387, doi:10.1364/AO.39.003380, (2000).
- 8 Cerussi, A. E. *et al.* Tissue phantoms in multicenter clinical trials for diffuse optical technologies. *Biomed Opt Express*. **3** (5), 966-971, doi:10.1364/BOE.3.000966, (2012).
- 9 Marín, N. M. *et al.* Calibration standards for multicenter clinical trials of fluorescence spectroscopy for in vivo diagnosis. *J Biomed Opt*. **11** (1), 014010, doi:10.1117/1.2166389, (2006).
- 10 Alexandrakis, G., Rannou, F. R., Chatziioannou, A. F. Tomographic bioluminescence imaging by use of a combined optical-PET (OPET) system: a computer simulation feasibility study. *Phys Med Biol*. **50** (17), 4225-4241 (2005).
- 11 Wan, Q., Beier, H. T., Ibey, B. L., Good, T., Coté, G. L. in *Optical Diagnostics and Sensing VII*. eds Gerard L. Coté & Alexander V. Priezzhev) 64450J (SPIE).
- 12 Chen, C. *et al.* Preparation of a skin equivalent phantom with interior micron-scale vessel structures for optical imaging experiments. *Biomed Opt Express*. **5** (9), 3140-3149, doi:10.1364/BOE.5.003140, (2014).
- 13 Pogue, B. W., Patterson, M. S. Review of tissue simulating phantoms for optical spectroscopy, imaging and dosimetry. *J Biomed Opt*. **11** (4), 041102, doi:10.1117/1.2335429, (2006).
- 14 Wróbel, M. S. *et al.* Use of optical skin phantoms for preclinical evaluation of laser efficiency for skin lesion therapy. *J Biomed Opt*. **20** (8), 085003, doi:10.1117/1.JBO.20.8.085003, (2015).
- 15 Cubeddu, R., Pifferi, A., Taroni, P., Torricelli, A., Valentini, G. A solid tissue phantom for photon migration studies. *Phys Med Biol*. **42** (10), 1971-1979 (1997).

573 16 Bae, Y., Son, T., Park, J., Jung, B. Fabrication of a thin-layer solid optical tissue phantom by  
574 a spin-coating method: pilot study. *J Biomed Opt.* **18** (2), 025006,  
575 doi:10.1117/1.JBO.18.2.025006, (2013).

576 17 Park, J. *et al.* in *Design and Performance Validation of Phantoms Used in Conjunction with*  
577 *Optical Measurement of Tissue V.* (ed Robert J. Nordstrom) 85830G (SPIE).

578 18 Luu, L., Roman, P. A., Mathews, S. A., Ramella-Roman, J. C. Microfluidics based phantoms  
579 of superficial vascular network. *Biomed Opt Express.* **3** (6), 1350-1364,  
580 doi:10.1364/BOE.3.001350, (2012).

581 19 Chen, A. I. *et al.* Multilayered tissue mimicking skin and vessel phantoms with tunable  
582 mechanical, optical, and acoustic properties. *Med Phys.* **43** (6Part1), 3117-3131,  
583 doi:10.1118/1.4951729, (2016).

584 20 Lurie, K. L., Smith, G. T., Khan, S. A., Liao, J. C., Ellerbee, A. K. Three-dimensional,  
585 distendable bladder phantom for optical coherence tomography and white light  
586 cystoscopy. *J Biomed Opt.* **19** (3), 036009, doi:10.1117/1.JBO.19.3.036009, (2014).

587 21 Golabchi, A. *et al.* Refractive errors and corrections for OCT images in an inflated lung  
588 phantom. *Biomed Opt Express.* **3** (5), 1101-1109, doi:10.1364/BOE.3.001101, (2012).

589 22 Rengier, F. *et al.* 3D printing based on imaging data: review of medical applications. *Int J*  
590 *Comput Assist Radiol and Surg.* **5** (4), 335-341, doi:10.1007/s11548-010-0476-x, (2010).

591 23 Wang, J. *et al.* Three-dimensional printing of tissue phantoms for biophotonic imaging.  
592 *Opt Lett.* **39** (10), 3010-3013, doi:10.1364/OL.39.003010, (2014).

593 24 Ghassemi, P. *et al.* Evaluation of Mobile Phone Performance for Near-Infrared  
594 Fluorescence Imaging. *IEEE Trans Biomed Eng.* **64** (7), 1650-1653 (2017).

595 25 Bentz, B. Z., Chavan, A. V., Lin, D., Tsai, E. H. R., Webb, K. J. Fabrication and application of  
596 heterogeneous printed mouse phantoms for whole animal optical imaging. *Appl Opt.* **55**  
597 (2), 280-287, doi:10.1364/AO.55.000280, (2016).

598 26 Diep, P. *et al.* Three-dimensional printed optical phantoms with customized absorption  
599 and scattering properties. *Biomed Opt Express.* **6** (11), 4212-4220,  
600 doi:10.1364/BOE.6.004212, (2015).

601 27 Pogue, B. W., Patterson, M. S. Review of tissue simulating phantoms for optical  
602 spectroscopy, imaging and dosimetry. *Journal of Biomedical Optics.* **11** (4), 041102-  
603 041102-041116, doi:10.1117/1.2335429, (2006).

604 28 de Bruin, D. M. *et al.* Optical phantoms of varying geometry based on thin building blocks  
605 with controlled optical properties. *J Biomed Opt.* **15** (2), 025001-025001-025010,  
606 doi:10.1117/1.3369003, (2010).

607 29 Boyle, A. J. *et al.* In vitro performance of a shape memory polymer foam-coated coil  
608 embolization device. *Med Eng Phys.* **49**, 56-62, (2017).

609 30 Hwang, W., Singhal, P., Miller, M. W., Maitland, D. J. In Vitro Study of Transcatheter  
610 Delivery of a Shape Memory Polymer Foam Embolic Device for Treating Cerebral  
611 Aneurysms. *J Med Dev.* **7** (2), 020932-020932-020932, doi:10.1115/1.4024338, (2013).

612 31 Giampietro Sgaragli and Maria, F. Human Tuberculosis I. Epidemiology, Diagnosis and  
613 Pathogenetic Mechanisms. *Curr Med Chem.* **23** (25), 2836-2873,  
614 doi:http://dx.doi.org/10.2174/0929867323666160607222854, (2016).

615 32 Mufti, N., Kong, Y., Cirillo, J. D., Maitland, K. C. Fiber optic microendoscopy for preclinical  
616 study of bacterial infection dynamics. *Biomed Opt Express.* **2** (5), 1121-1134,

doi:10.1364/BOE.2.001121, (2011).

33 Nooshabadi, F. *et al.* Intravital fluorescence excitation in whole-animal optical imaging. *PLoS One*. **11** (2), e0149932, doi:10.1371/journal.pone.0149932, (2016).

34 Nooshabadi, F. *et al.* Intravital excitation increases detection sensitivity for pulmonary tuberculosis by whole-body imaging with beta-lactamase reporter enzyme fluorescence. *J Biophotonics*. doi:10.1002/jbio.201600132, (2016).

35 Duck, F. A. *Physical Properties of Tissue: A Comprehensive Reference Book*. (Academic Press, Inc., 1990).

36 Tuchin, V. V., Tuchin, V. *Tissue optics: light scattering methods and instruments for medical diagnosis*. Vol. 13 (SPIE press Bellingham, 2007).

37 Prah, S. Everything I think you should know about Inverse Adding-Doubling. (Oregon Tech, 2011).

38 Inverse Adding-Doubling v.3-9-12 (2014).

39 Link, T. M. *et al.* A Comparative Study of Trabecular Bone Properties in the Spine and Femur Using High Resolution MRI and CT. *J Bone Miner Res*. **13** (1), 122-132, doi:10.1359/jbmr.1998.13.1.122, (1998).

40 Batiste, D. L. *et al.* High-resolution MRI and micro-CT in an ex vivo rabbit anterior cruciate ligament transection model of osteoarthritis. *Osteoarthr cartil*. **12** (8), 614-626 (2004).

41 Greening, G. J. *et al.* Characterization of thin poly(dimethylsiloxane)-based tissue-simulating phantoms with tunable reduced scattering and absorption coefficients at visible and near-infrared wavelengths. *J Biomed Opt*. **19** (11), 115002, doi:10.1117/1.JBO.19.11.115002, (2014).

42 Meissner, S., Knels, L., Krueger, A., Koch, T., Koch, E. Simultaneous three-dimensional optical coherence tomography and intravital microscopy for imaging subpleural pulmonary alveoli in isolated rabbit lungs. *J Biomed Opt*. **14** (5), 054020, doi:10.1117/1.3247149, (2009).

43 Morris, A. H. *et al.* A new nuclear magnetic resonance property of lung. *J Appl Phys*. **58** (3), 759-762 (1985).

44 Hearon, K. *et al.* Porous Shape Memory Polymers. *Polym Rev (Phila Pa)*. **53** (1), 41-75, doi:10.1080/15583724.2012.751399, (2013).



Figure 1

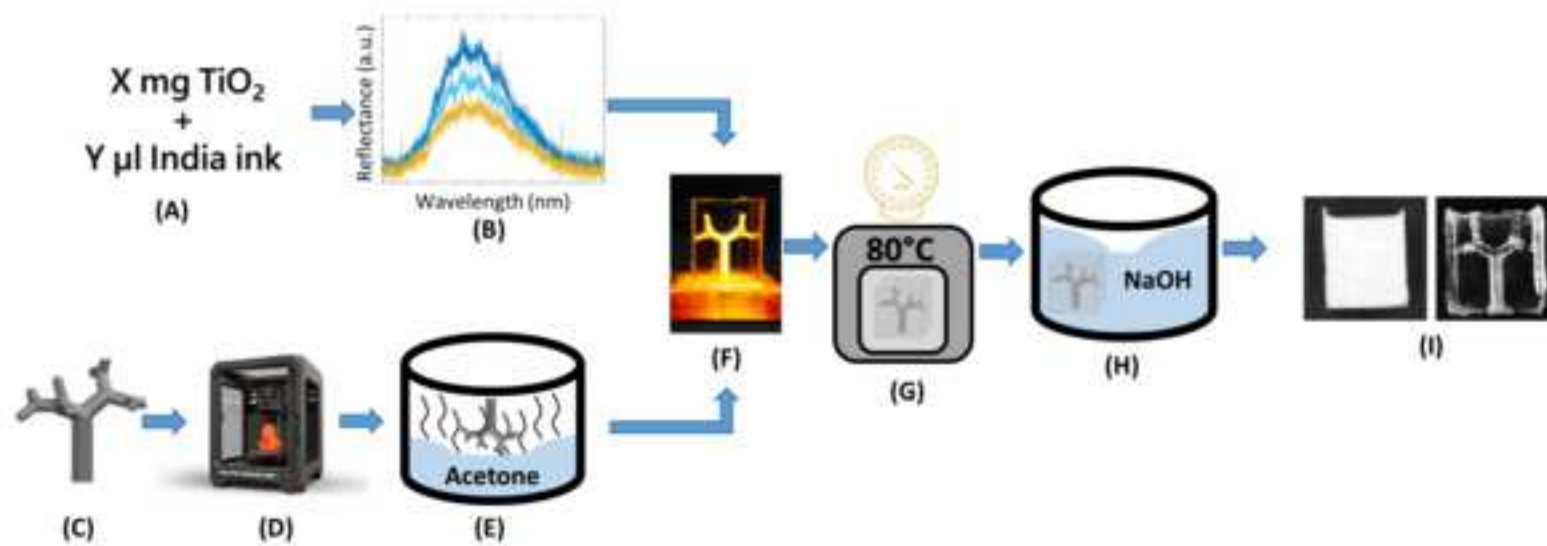


Figure 2

[Click here to download Figure Fig 2.tif](#)

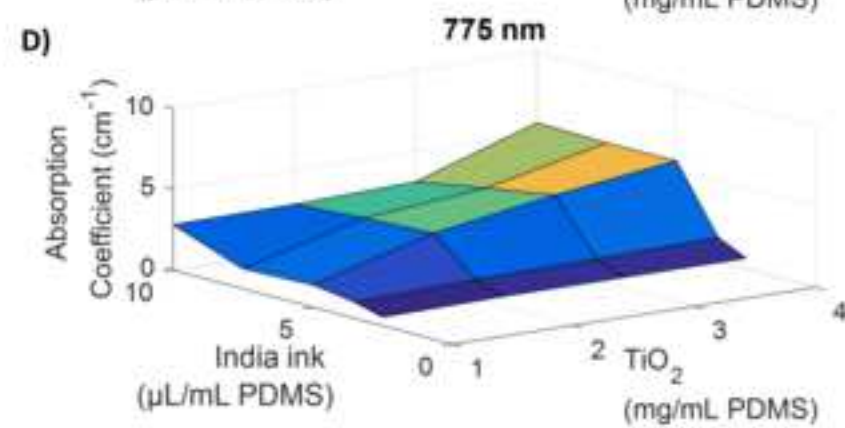
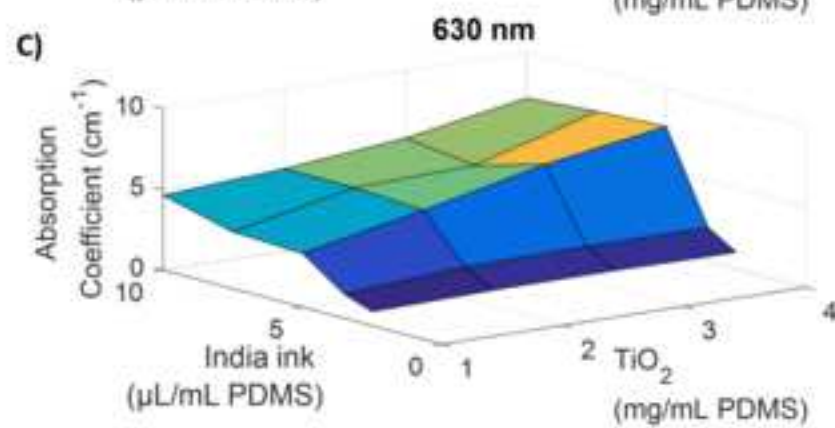
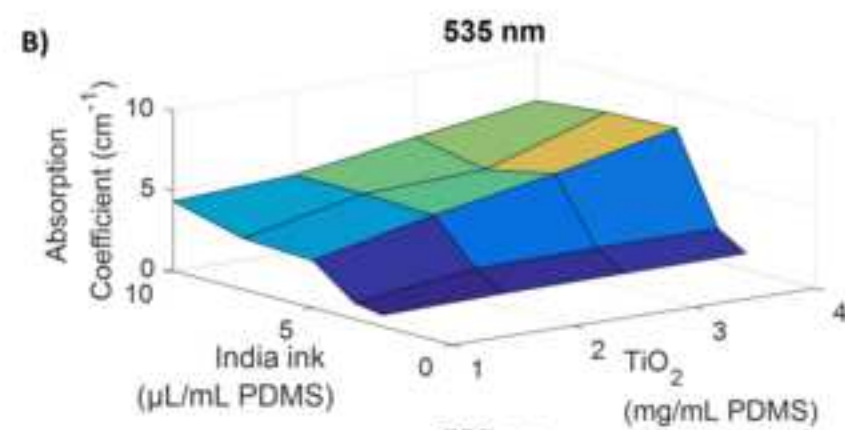
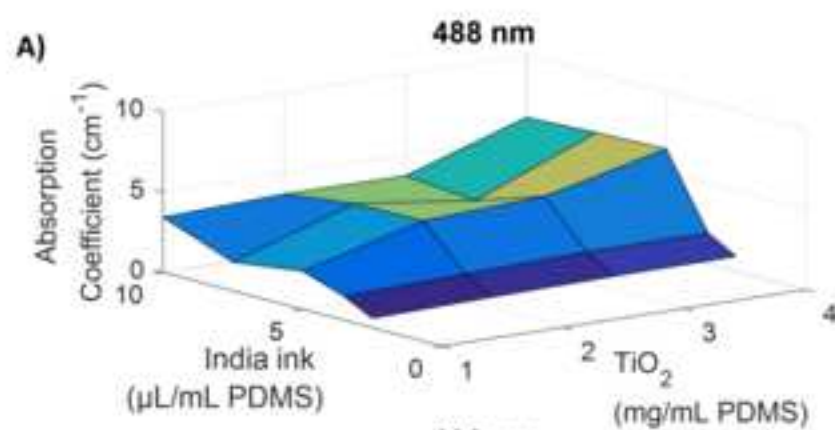
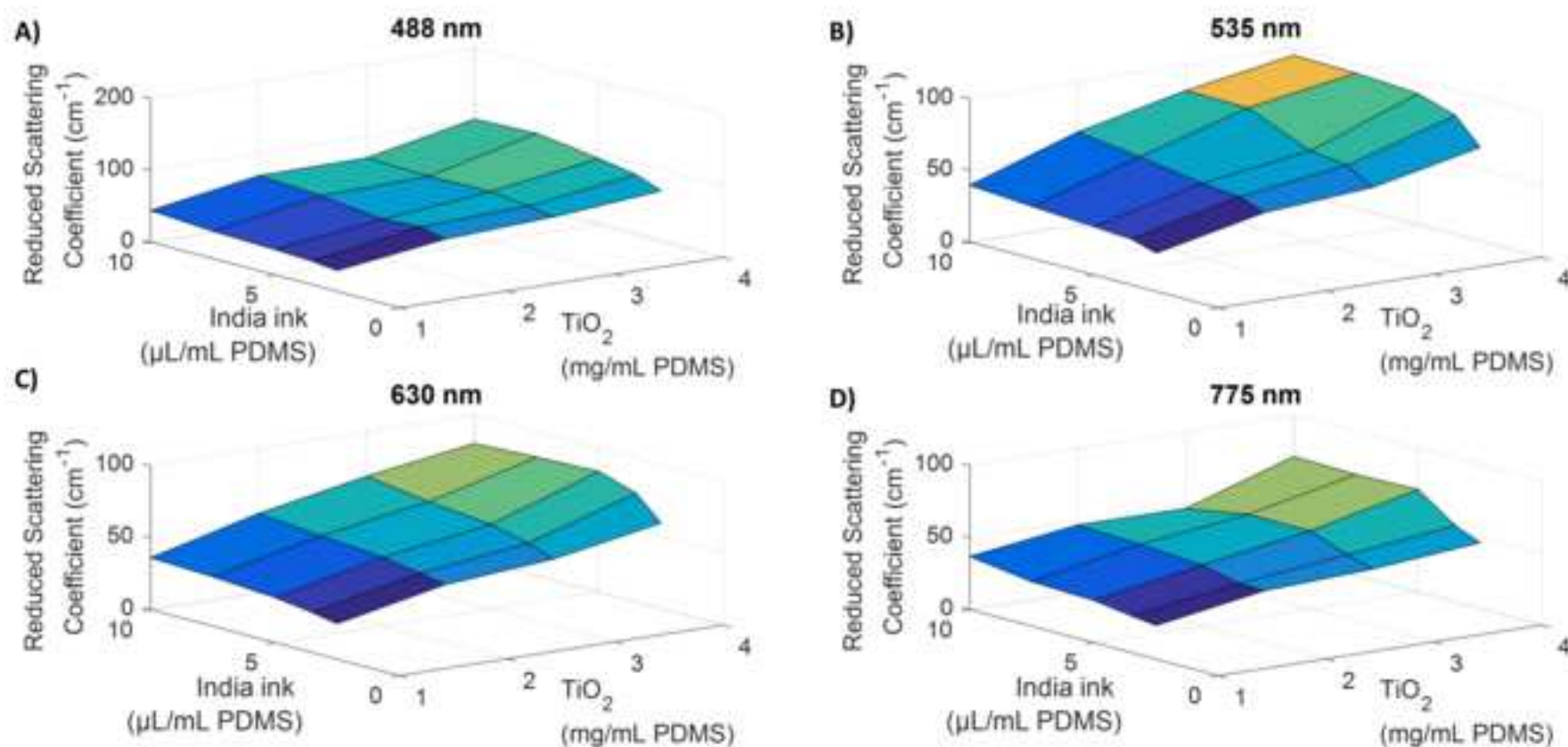


Figure 3

[Click here to download Figure Fig 3.tif](#)



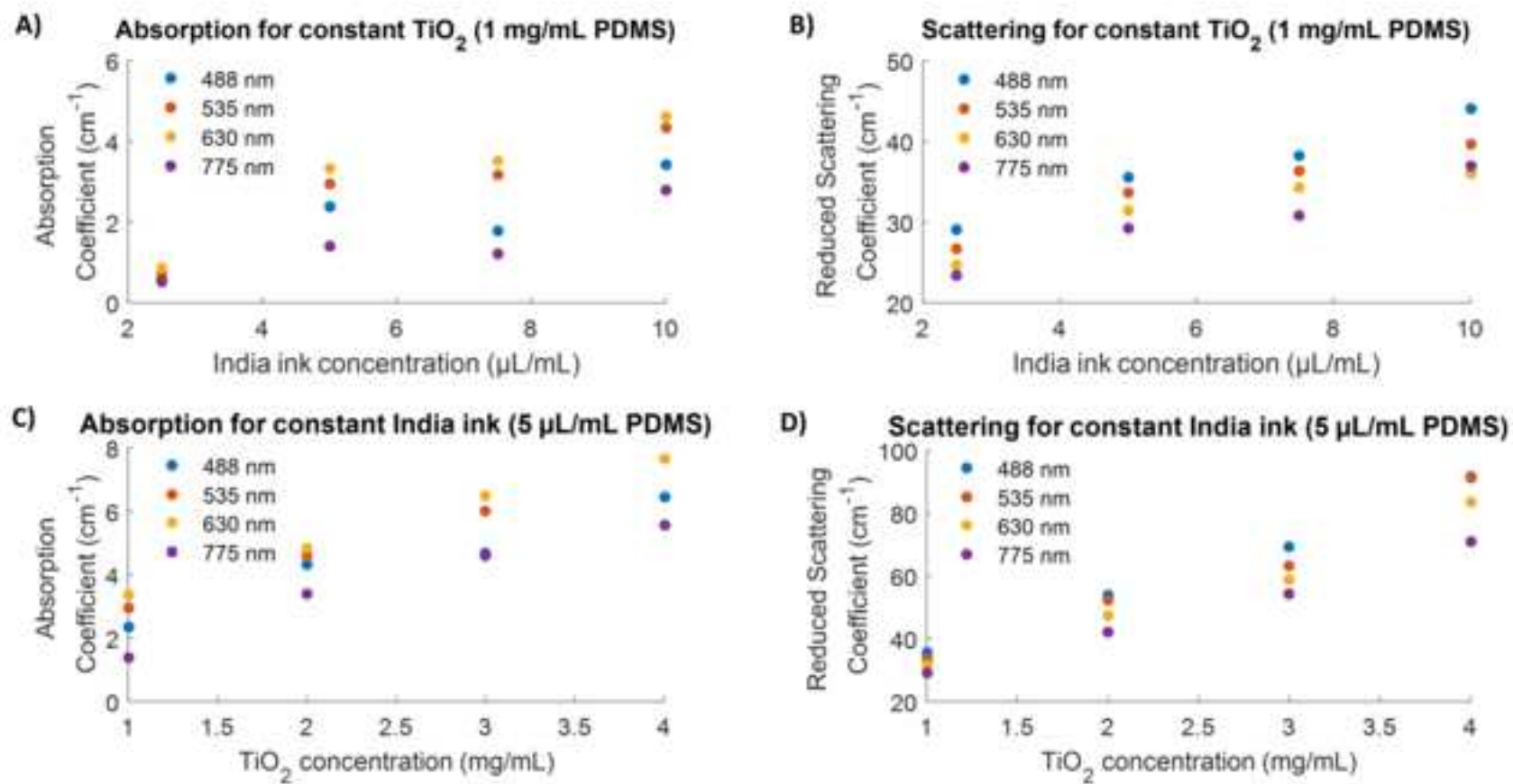
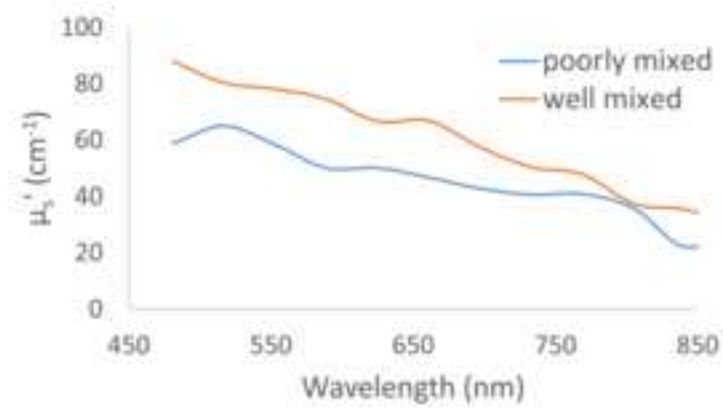


Figure 5



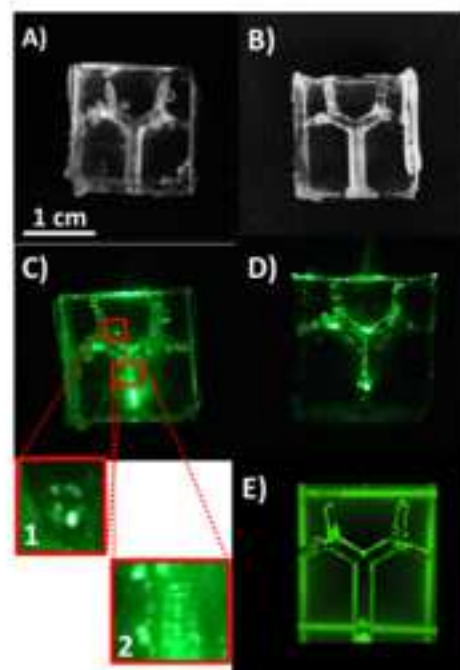
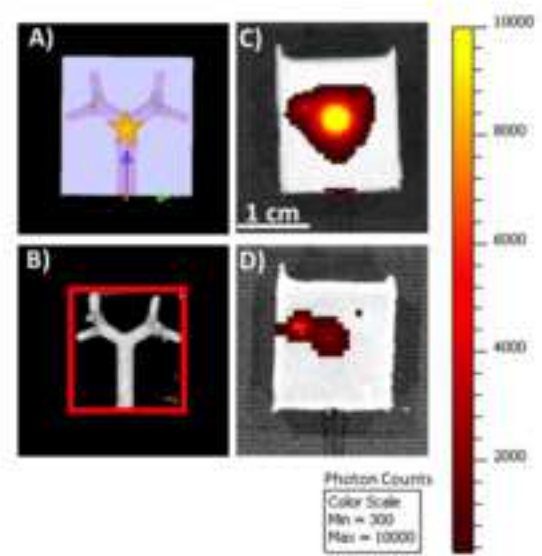


Figure 7



[illegible]



4.5	6.5
---	---
---	---
---	---
3 mg TiO <sub>2</sub> + 5 uL India ink	---
---	---
---	---
---	4 mg TiO <sub>2</sub> + 5 uL India ink

535 nm		$\mu_a$ ( cm <sup>-1</sup> )						
		0.5	1	2	3	4.5	6	7
$\mu_s'$ (cm <sup>-1</sup> )	30	1 mg TiO <sub>2</sub> + 2.5 uL India ink	---	---	1 mg TiO <sub>2</sub> + 5 uL India ink	---	---	---
	40	---	2 mg TiO <sub>2</sub> + 2.5 uL India ink	---	1 mg TiO <sub>2</sub> + 7.5 uL India ink	1 mg TiO <sub>2</sub> + 10 uL India ink	---	---
	50	---	---	2 mg TiO <sub>2</sub> + 3.5 uL India ink	---	2 mg TiO <sub>2</sub> + 5 uL India ink	---	---
	70	---	4 mg TiO <sub>2</sub> + 2.5 uL India ink	---	---	3 mg TiO <sub>2</sub> + 5 uL India ink	---	---
	80	---	---	4 mg TiO <sub>2</sub> + 3.5 uL India ink	---	3 mg TiO <sub>2</sub> + 7.5 uL India ink	3 mg TiO <sub>2</sub> + 10 uL India ink	---
	90	---	---	---	---	---	---	4 mg TiO <sub>2</sub> + 10 uL India ink

630 nm		$\mu_a$ (cm <sup>-1</sup> )						
		1	2	3.5	4.5	5	6	6.5
$\mu_s'$ (cm <sup>-1</sup> )	20	1 mg TiO <sub>2</sub> + 2.5 uL India ink	---	---	---	---	---	---
	30	---	---	1 mg TiO <sub>2</sub> + 7.5 uL India ink	---	---	---	---
	40	2 mg TiO <sub>2</sub> + 2.5 uL India ink	2 mg TiO <sub>2</sub> + 3.5 uL India ink	---	1 mg TiO <sub>2</sub> + 10 uL India ink	---	---	---
	50	---	---	---	---	2 mg TiO <sub>2</sub> + 5 uL India ink	---	---
	60	4 mg TiO <sub>2</sub> + 2.5 uL India ink	---	---	---	3 mg TiO <sub>2</sub> + 7.5 uL India ink	---	3 mg TiO <sub>2</sub> + 5 uL India ink
	70	---	---	---	---	---	3 mg TiO <sub>2</sub> + 10 uL India ink	---
	80	---	4 mg TiO <sub>2</sub> + 3.5 uL India ink	---	---	---	---	---

7
---
---
---
---
---
---
4 mg TiO <sub>2</sub> + 10 uL India ink

775 nm		$\mu_a \text{ ( cm}^{-1}\text{)}$						
		0.5	1	1.5	3	3.5	4.5	5.5
$\mu_s' \text{ ( cm}^{-1}\text{)}$	20	1 mg TiO <sub>2</sub> + 2.5 uL India ink	---	---	---	---	---	---
	30	---	1 mg TiO <sub>2</sub> + 7.5 uL India ink	1 mg TiO <sub>2</sub> + 5 uL India ink	---	---	---	---
	40	2 mg TiO <sub>2</sub> + 2.5 uL India ink	2 mg TiO <sub>2</sub> + 3.5 uL India ink	---	1 mg TiO <sub>2</sub> + 10 uL India ink	2 mg TiO <sub>2</sub> + 5 uL India ink	---	---
	50	4 mg TiO <sub>2</sub> + 2.5 uL India ink	---	4 mg TiO <sub>2</sub> + 3.5 uL India ink	3 mg TiO <sub>2</sub> + 10 uL India ink	3 mg TiO <sub>2</sub> + 7.5 uL India ink	3 mg TiO <sub>2</sub> + 5 uL India ink	---
	70	---	---	---	---	---	---	4 mg TiO <sub>2</sub> + 5 uL India ink

6
---
---
---
---
4 mg TiO <sub>2</sub> + 10 uL India ink

	Absorption Coefficient (cm <sup>-1</sup> )	Reduced Scattering Coefficient (cm <sup>-1</sup> )
Healthy mouse lung tissue	2.05 ± 0.58	52.69 ± 7.83
Healthy phantom <sup>(2)</sup> <i>mg TiO<sub>2</sub> + 3.5 µL India ink</i>	1.96 ± 0.699	49.66 ± .12
Inflamed mouse lung tissue	5.49 ± 1.32	38.94 ± 9.68
Inflamed phantom <sup>(1)</sup> <i>mg TiO<sub>2</sub> + 10 µL India ink</i>	4.34 ± 0.873	39.56 ± 5.02

	Base diameter (mm)	Distal branch diameter (mm)
Solid model	2.7	1.38
Vapor polished print	2.56 ± 0.026	1.38 ± 0.141
PDMS mold (measured from CT)	2.55 ± 0.021	1.39± 0.055



Name of Material/ Equipment	Company	Catalog Number
Dow Corning Sylgard 184 Silicone Encapsulant Clear 0.5 kg Kit	Ellsworth Adhesives	184 SIL ELAST KIT 0.5KG
White Rutile Titanium Dioxide powder	Atlantic Equipment Engineers	TI-602
Higgins Fountain Pen India Ink	Michaels Craft Stores	10015483
Heat Resistant tape	Uline	S-7595
Fortus 360mc 3D printer	Stratasys	N/A
ABS Ivory Model Material	Stratasys	SDS-000001
SR-30 Soluble Support	Stratasys	400638-0001
Flacktek Speedmixer	Flacktek Inc.	DAC 150.1 FV
Integrating sphere	Edmund Optics	58-585
Polycarbonate build plates (1 mm)	Stratasys	N/A

<b>Comments/Description</b>
Polydimethylsiloxane: polymer base for optical phantoms
Scattering particles for optical phantoms
Absorbing particles for optical phantom
Heat resistant tape for polymer molds
Able to switch build and support material with this model printer
Material for printing mold parts and/or using as support for printing internal structure
Base soluble support material for printing internal structure
For efficient mixing of polymer and particles
For measuring optical properties
Used polycarbonate build plates from Stratasys printer can also be used



1 Alewife Center #200  
Cambridge, MA 02140  
tel. 617.945.9051  
www.jove.com

## ARTICLE AND VIDEO LICENSE AGREEMENT

Title of Article: Fabrication and characterization of optical tissue phantoms containing macrostructure

Author(s): M. Durkee, L. Nash, F. Nooshabadi, J. Cirillo, D. Maitland, K. Maitland

Item 1 (check one box): The Author elects to have the Materials be made available (as described at <http://www.jove.com/author>) via: ☒ Standard Access ☐ Open Access

Item 2 (check one box):

- ☒ The Author is NOT a United States government employee.
- ☐ The Author is a United States government employee and the Materials were prepared in the course of his or her duties as a United States government employee.
- ☐ The Author is a United States government employee but the Materials were NOT prepared in the course of his or her duties as a United States government employee.

### ARTICLE AND VIDEO LICENSE AGREEMENT

1. **Defined Terms.** As used in this Article and Video License Agreement, the following terms shall have the following meanings: “**Agreement**” means this Article and Video License Agreement; “**Article**” means the article specified on the last page of this Agreement, including any associated materials such as texts, figures, tables, artwork, abstracts, or summaries contained therein; “**Author**” means the author who is a signatory to this Agreement; “**Collective Work**” means a work, such as a periodical issue, anthology or encyclopedia, in which the Materials in their entirety in unmodified form, along with a number of other contributions, constituting separate and independent works in themselves, are assembled into a collective whole; “**CRC License**” means the Creative Commons Attribution-Non Commercial-No Derivs 3.0 Unported Agreement, the terms and conditions of which can be found at: <http://creativecommons.org/licenses/by-nc-nd/3.0/legalcode>; “**Derivative Work**” means a work based upon the Materials or upon the Materials and other pre-existing works, such as a translation, musical arrangement, dramatization, fictionalization, motion picture version, sound recording, art reproduction, abridgment, condensation, or any other form in which the Materials may be recast, transformed, or adapted; “**Institution**” means the institution, listed on the last page of this Agreement, by which the Author was employed at the time of the creation of the Materials; “**JoVE**” means MyJoVE Corporation, a Massachusetts corporation and the publisher of *The Journal of Visualized Experiments*; “**Materials**” means the Article and / or the Video; “**Parties**” means the Author and JoVE; “**Video**” means any video(s) made by the Author, alone or in conjunction with any other parties, or by JoVE or its affiliates or agents, individually or in collaboration with the Author or any other parties, incorporating all or any portion of the Article, and in which the Author may or may not appear.

2. **Background.** The Author, who is the author of the Article, in order to ensure the dissemination and protection of the Article, desires to have the JoVE publish the Article and create and transmit videos based on the Article. In furtherance of such goals, the Parties desire to memorialize in this Agreement the respective rights of each Party in and to the Article and the Video.

3. **Grant of Rights in Article.** In consideration of JoVE agreeing to publish the Article, the Author hereby grants to JoVE, subject to **Sections 4 and 7** below, the exclusive, royalty-free, perpetual (for the full term of copyright in the Article, including any extensions thereto) license (a) to publish, reproduce, distribute, display and store the Article in all forms, formats and media whether now known or hereafter developed (including without limitation in print, digital and electronic form) throughout the world, (b) to translate the Article into other languages, create adaptations, summaries or extracts of the Article or other Derivative Works (including, without limitation, the Video) or Collective Works based on all or any portion of the Article and exercise all of the rights set forth in (a) above in such translations, adaptations, summaries, extracts, Derivative Works or Collective Works and (c) to license others to do any or all of the above. The foregoing rights may be exercised in all media and formats, whether now known or hereafter devised, and include the right to make such modifications as are technically necessary to exercise the rights in other media and formats. If the “Open Access” box has been checked in **Item 1** above, JoVE and the Author hereby grant to the public all such rights in the Article as provided in, but subject to all limitations and requirements set forth in, the CRC License.

## ARTICLE AND VIDEO LICENSE AGREEMENT

4. Retention of Rights in Article. Notwithstanding the exclusive license granted to JoVE in **Section 3** above, the Author shall, with respect to the Article, retain the non-exclusive right to use all or part of the Article for the non-commercial purpose of giving lectures, presentations or teaching classes, and to post a copy of the Article on the Institution's website or the Author's personal website, in each case provided that a link to the Article on the JoVE website is provided and notice of JoVE's copyright in the Article is included. All non-copyright intellectual property rights in and to the Article, such as patent rights, shall remain with the Author.

5. Grant of Rights in Video – Standard Access. This **Section 5** applies if the "Standard Access" box has been checked in **Item 1** above or if no box has been checked in **Item 1** above. In consideration of JoVE agreeing to produce, display or otherwise assist with the Video, the Author hereby acknowledges and agrees that, Subject to **Section 7** below, JoVE is and shall be the sole and exclusive owner of all rights of any nature, including, without limitation, all copyrights, in and to the Video. To the extent that, by law, the Author is deemed, now or at any time in the future, to have any rights of any nature in or to the Video, the Author hereby disclaims all such rights and transfers all such rights to JoVE.

6. Grant of Rights in Video – Open Access. This **Section 6** applies only if the "Open Access" box has been checked in **Item 1** above. In consideration of JoVE agreeing to produce, display or otherwise assist with the Video, the Author hereby grants to JoVE, subject to **Section 7** below, the exclusive, royalty-free, perpetual (for the full term of copyright in the Article, including any extensions thereto) license (a) to publish, reproduce, distribute, display and store the Video in all forms, formats and media whether now known or hereafter developed (including without limitation in print, digital and electronic form) throughout the world, (b) to translate the Video into other languages, create adaptations, summaries or extracts of the Video or other Derivative Works or Collective Works based on all or any portion of the Video and exercise all of the rights set forth in (a) above in such translations, adaptations, summaries, extracts, Derivative Works or Collective Works and (c) to license others to do any or all of the above. The foregoing rights may be exercised in all media and formats, whether now known or hereafter devised, and include the right to make such modifications as are technically necessary to exercise the rights in other media and formats. For any Video to which this Section 6 is applicable, JoVE and the Author hereby grant to the public all such rights in the Video as provided in, but subject to all limitations and requirements set forth in, the CRC License.

7. Government Employees. If the Author is a United States government employee and the Article was prepared in the course of his or her duties as a United States government employee, as indicated in **Item 2** above, and any of the licenses or grants granted by the Author hereunder exceed the scope of the 17 U.S.C. 403, then the rights granted hereunder shall be limited to the maximum rights permitted under such

statute. In such case, all provisions contained herein that are not in conflict with such statute shall remain in full force and effect, and all provisions contained herein that do so conflict shall be deemed to be amended so as to provide to JoVE the maximum rights permissible within such statute.

8. Likeness, Privacy, Personality. The Author hereby grants JoVE the right to use the Author's name, voice, likeness, picture, photograph, image, biography and performance in any way, commercial or otherwise, in connection with the Materials and the sale, promotion and distribution thereof. The Author hereby waives any and all rights he or she may have, relating to his or her appearance in the Video or otherwise relating to the Materials, under all applicable privacy, likeness, personality or similar laws.

9. Author Warranties. The Author represents and warrants that the Article is original, that it has not been published, that the copyright interest is owned by the Author (or, if more than one author is listed at the beginning of this Agreement, by such authors collectively) and has not been assigned, licensed, or otherwise transferred to any other party. The Author represents and warrants that the author(s) listed at the top of this Agreement are the only authors of the Materials. If more than one author is listed at the top of this Agreement and if any such author has not entered into a separate Article and Video License Agreement with JoVE relating to the Materials, the Author represents and warrants that the Author has been authorized by each of the other such authors to execute this Agreement on his or her behalf and to bind him or her with respect to the terms of this Agreement as if each of them had been a party hereto as an Author. The Author warrants that the use, reproduction, distribution, public or private performance or display, and/or modification of all or any portion of the Materials does not and will not violate, infringe and/or misappropriate the patent, trademark, intellectual property or other rights of any third party. The Author represents and warrants that it has and will continue to comply with all government, institutional and other regulations, including, without limitation all institutional, laboratory, hospital, ethical, human and animal treatment, privacy, and all other rules, regulations, laws, procedures or guidelines, applicable to the Materials, and that all research involving human and animal subjects has been approved by the Author's relevant institutional review board.

10. JoVE Discretion. If the Author requests the assistance of JoVE in producing the Video in the Author's facility, the Author shall ensure that the presence of JoVE employees, agents or independent contractors is in accordance with the relevant regulations of the Author's institution. If more than one author is listed at the beginning of this Agreement, JoVE may, in its sole discretion, elect not take any action with respect to the Article until such time as it has received complete, executed Article and Video License Agreements from each such author. JoVE reserves the right, in its absolute and sole discretion and without giving any reason therefore, to accept or decline any work submitted to JoVE. JoVE and its employees, agents and independent contractors shall have

## ARTICLE AND VIDEO LICENSE AGREEMENT

full, unfettered access to the facilities of the Author or of the Author's institution as necessary to make the Video, whether actually published or not. JoVE has sole discretion as to the method of making and publishing the Materials, including, without limitation, to all decisions regarding editing, lighting, filming, timing of publication, if any, length, quality, content and the like.

11. **Indemnification.** The Author agrees to indemnify JoVE and/or its successors and assigns from and against any and all claims, costs, and expenses, including attorney's fees, arising out of any breach of any warranty or other representations contained herein. The Author further agrees to indemnify and hold harmless JoVE from and against any and all claims, costs, and expenses, including attorney's fees, resulting from the breach by the Author of any representation or warranty contained herein or from allegations or instances of violation of intellectual property rights, damage to the Author's or the Author's institution's facilities, fraud, libel, defamation, research, equipment, experiments, property damage, personal injury, violations of institutional, laboratory, hospital, ethical, human and animal treatment, privacy or other rules, regulations, laws, procedures or guidelines, liabilities and other losses or damages related in any way to the submission of work to JoVE, making of videos by JoVE, or publication in JoVE or elsewhere by JoVE. The Author shall be responsible for, and shall hold JoVE harmless from, damages caused by lack of sterilization, lack of cleanliness or by contamination due to the making of a video by JoVE its employees, agents or independent contractors. All sterilization, cleanliness or decontamination procedures shall be solely the responsibility of the Author and shall be undertaken at the Author's


expense. All indemnifications provided herein shall include JoVE's attorney's fees and costs related to said losses or damages. Such indemnification and holding harmless shall include such losses or damages incurred by, or in connection with, acts or omissions of JoVE, its employees, agents or independent contractors.

12. **Fees.** To cover the cost incurred for publication, JoVE must receive payment before production and publication the Materials. Payment is due in 21 days of invoice. Should the Materials not be published due to an editorial or production decision, these funds will be returned to the Author. Withdrawal by the Author of any submitted Materials after final peer review approval will result in a US\$1,200 fee to cover pre-production expenses incurred by JoVE. If payment is not received by the completion of filming, production and publication of the Materials will be suspended until payment is received.

13. **Transfer, Governing Law.** This Agreement may be assigned by JoVE and shall inure to the benefits of any of JoVE's successors and assignees. This Agreement shall be governed and construed by the internal laws of the Commonwealth of Massachusetts without giving effect to any conflict of law provision thereunder. This Agreement may be executed in counterparts, each of which shall be deemed an original, but all of which together shall be deemed to me one and the same agreement. A signed copy of this Agreement delivered by facsimile, e-mail or other means of electronic transmission shall be deemed to have the same legal effect as delivery of an original signed copy of this Agreement.

A signed copy of this document must be sent with all new submissions. Only one Agreement required per submission.

### CORRESPONDING AUTHOR:

Name: Kristen Maitland  
Department: Biomedical Engineering  
Institution: Texas A&M University  
Article Title: Fabrication and characterization of optical tissue phantoms containing macrostructure  
Signature:  Date: 7/17/17

Please submit a signed and dated copy of this license by one of the following three methods:

- 1) Upload a scanned copy of the document as a pdf on the JoVE submission site;
- 2) Fax the document to +1.866.381.2236;
- 3) Mail the document to JoVE / Attn: JoVE Editorial / 1 Alewife Center #200 / Cambridge, MA 02139

For questions, please email [submissions@jove.com](mailto:submissions@jove.com) or call +1.617.945.9051

Journal of Visualized Experiments

Manuscript # JoVE57031

Fabrication and characterization of optical tissue phantoms containing macrostructure

## Editorial and Peer Review Comments and Response

We thank the editors and reviewers for the constructive comments to revise the manuscript. We have addressed each comment in the manuscript, as appropriate, and in this response. All referenced page numbers and lines are from the version submitted with track changes on.

### Editorial comments:

1. Please take this opportunity to thoroughly proofread the manuscript to ensure that there are no spelling or grammar issues. The JoVE editor will not copy-edit your manuscript and any errors in the submitted revision may be present in the published version.

**Completed.**

2. Please move detailed discussion of results (from the Long Abstract, Introduction, and Discussion) to the Representative Results section.

**Completed.**

3. (Please print and sign the attached Author License Agreement (ALA). Please then scan and upload the signed ALA with the manuscript files to your Editorial Manager account.)

**The ALA document was signed and uploaded with the first submission.**

4. Please define all abbreviations before use, like  $\mu$ s and  $\mu$ a (See Tables 1–4).

**Definitions for the terms in the tables have been added to page 4, lines 138-139.**

5. Protocol: Please ensure that all text in the protocol section is written in the imperative tense as if telling someone how to do the technique (e.g., “Do this,” “Ensure that,” etc.). (The actions should be described in the imperative tense in complete sentences wherever possible.) Avoid usage of phrases such as “could be,” “should be,” and “would be” throughout the Protocol. Any text that cannot be written in the imperative tense may be added as a “Note.” (However, notes should be concise and used sparingly.) (Please include all safety procedures and use of hoods, etc.)

**All non-imperative language has been replaced in the protocol. Changes were made to step 1.1 (page 4, line 133), step 2.4.3 (page 6, line 238), and step 3 (pages 6, lines 256-258).**

6. Protocol: Please add more details to your protocol steps. Please ensure you answer the “how” question, i.e., how is the step performed? Alternatively, add references to published material specifying how to perform the protocol action.

**Completed.**

7. Protocol: Please ensure any steps requiring particular caution are noted as such.

**“CAUTION” was added to step 2.4.3.**

8. 1.3.1: How much PDMS should be used?

**More information has been added to step 1.3.1 to account for the amount of PDMS used for these standards and the two recipes verified in this step. (page 4, lines 149-152)**

9. 1.3.3: Where will the mixture be poured?

**The mixture can be poured into any vessel or container; we have added a suggested vessel to pour the PDMS into on page 4, line 158.**

10. 1.3.4: What will be used to degas the slabs?

**A clarification on what equipment is used to degas has been added to page 4, line 161.**

11. 1.5: Please provide more detail about the use of this software; i.e., specific steps the user should do to carry out the analysis.

**The IAD software has a full manual that comes with the download. More details have been added to the manuscript about where to run the software from and the output file (page 5, lines 202-207). However, thorough detail on running this software is dependent on the user and storage on their personal computer. A sample version of the IAD input file is included as Supplemental Material 1 and referenced on page 5, line 202.**

12. 2.1: Please provide more information about the design process, or a citation. Also, can you provide the CAD file you used here or a citation for it?

**More detail on this design was provided in the introduction on page 3, lines 116-119. Also, a generalizing statement about the internal structure has been added to step 2.1 (page 5, lines 218-219), and the .stl file is included as Supplemental Material 2 and referenced on page 5, lines 215-216.**

13. 2.2: What is the dissolvable part?

**The dissolvable part is the object that comes out of the 3D printer. A clarification has been added to page 5, lines 222-223.**

14. 2.5: How exactly will you verify the geometry?

**Verification of the geometry should be done by comparing measurements of the vapor polished, dissolvable printed part to the measurements used in the solid model design. This step is used to ensure that the vapor polishing did not alter the part significantly from the design of the solid model. A short clarification has also been added to page 6, line 245.**

15. 3: Please provide more detail in this section (e.g., about the printing process, where the sheets go, how the base plate is placed inside, etc.), or citations.

**Step 3 and its sub-steps have been edited to include more specific details about the fabrication of the PDMS mold (pages 6-7, lines 260-263 and 275-278).**

16. 4.1–4.3: Many of these details could be in step 1 instead, especially given that it is intended to be filmed.

**Given that the amount of PDMS made is different for the slabs and the full phantoms, more information was added to step 1.3.1. See response to Editorial comment 8.**



17. 4.4: Around how much time total should this take?

**The timing of this step varies depending on the internal geometry used, the size of the part, and the height of the mold sidings. An irregular part inside of the mold can cause air to be trapped in the PDMS, so if there are many bubbles, degassing the PDMS will cause the level to rise, sometimes spilling over the mold sidings. Once the large bubbles are out of solution, the phantom can be left to degas without blowing off the top layer of bubbles. A general statement about the timing of the initial iterative process of degassing has been added to page 7, lines 301-302.**

18. 4.7: What concentration of NaOH?

**The molarity of the bath is ~0.5 M. This detail has been added to the manuscript (page 8, line 309).**

19. 5.1: Please provide more detail for this step (especially what you intend to film, exactly), or a citation.

**The verification of phantom fabrication step is similar to step 2.5. However, because the designed part is now a void within the PDMS, it is not possible to directly measure it without imaging the phantom. The imaging is meant to ensure that 1) the printed part is fully dissolved and 2) the geometry is still on the same scale and shape as the original design of the solid model. A clarification has been added to page 8, lines 327-328.**

20. Protocol: There is a 10 page limit for the Protocol, but there is a 2.75 page limit for filmable content. Please highlight 2.75 pages or less of the Protocol (including headings and spacing) that identifies the essential steps of the protocol for the video, i.e., the steps that should be visualized to tell the most cohesive story of the Protocol. Remember that non-highlighted Protocol steps will remain in the manuscript, and therefore will still be available to the reader.

**The highlighted sections were reviewed to best represent the critical steps in the protocol.**

21. Figure 4: Counts of what? Also, please indicate the wavelength in the Legend.

**The figure legend has been updated to read “photon counts”. An additional statement of the illumination wavelength was also added to the Figure 7 (previously figure 4) caption.**

22. Please ensure that the references appear as the following: [Lastname, F.I., LastName, F.I., LastName, F.I. Article Title. Source. Volume (Issue), FirstPage – LastPage, doi: DOI (YEAR).]

**The bibliographic style has been updated to exclude the ampersand before the final author.**

#### **Reviewers' comments:**

##### **Reviewer #1:**

Manuscript Summary:

This is an interesting study that has significant implication in the development of optical imaging devices. Recommended for publication after the authors address the following major concerns below.

##### **Major Concerns:**

1. The review of literature is missing some key relevant studies; this seems to indicate a surprising lack of knowledge regarding phantom fabrication approaches which should be addressed.



- a. In spite of using 3D printing to generate optical phantom molds, prior papers which have implemented 3D printers to generate optical phantoms are not mentioned (e.g., Wang et al., *Optics Letters* 2014, Diep et al., *Biomed Opt Exp* 2015, Bentz et al., *Appl Opt* 2016, etc.).
- b. Furthermore, given the manuscript's stated need for phantoms with "spatially complex tissue where three dimensional structures, such as blood vessels" the paper fails to note that prior studies that have already detailed the fabrication and implementation of optical phantoms with irregular, image-defined vascular structures using 3D printing (Ghassemi et al., *JBO* 2015, Ghassemi et al., *IEEE TBME* 2017).
- c. The authors should add relevant papers and justify why a mold-based approach to generating complex structures was taken rather than the direct 3D-printing approaches described in relevant prior studies - particularly in light of the fact that modern 3D printers which can accommodate the addition of chromophores and scattering particles.

**We appreciate the reviewer identifying this omission. An in-depth review of 3D printing as a phantom fabrication method, both as a mold and for the phantom itself, has been added to the introduction to better frame the protocol presented in this paper. (page 3, lines 95-109). The reviewer's suggestions for references have been added, along with other references on 3D printed phantoms. References have also been added to the statement quoted above in 1.b (page 2, line 87). The materials currently used for 3D printing limit the tunability of optical properties because the base materials are usually not optically clear. By molding with PDMS, we can achieve a greater range of optical properties, mainly lower scattering coefficients, when desired. This was also addressed in the additional paragraph added to the introduction.**

#### **References added:**

- 18 Luu, L., Roman, P. A., Mathews, S. A., Ramella-Roman, J. C. Microfluidics based phantoms of superficial vascular network. *Biomedical Optics Express*. **3** (6), 1350-1364, doi:10.1364/BOE.3.001350, (2012).
- 19 Chen, A. I. *et al.* Multilayered tissue mimicking skin and vessel phantoms with tunable mechanical, optical, and acoustic properties. *Medical Physics*. **43** (6Part1), 3117-3131, doi:10.1118/1.4951729, (2016).
- 22 Rengier, F. *et al.* 3D printing based on imaging data: review of medical applications. *International Journal of Computer Assisted Radiology and Surgery*. **5** (4), 335-341, doi:10.1007/s11548-010-0476-x, (2010).
- 23 Wang, J. *et al.* Three-dimensional printing of tissue phantoms for biophotonic imaging. *Optics Letters*. **39** (10), 3010-3013, doi:10.1364/OL.39.003010, (2014).
- 24 Ghassemi, P. *et al.* Evaluation of Mobile Phone Performance for Near-Infrared Fluorescence Imaging. *IEEE Transactions on Biomedical Engineering*. **64** (7), 1650-1653 (2017).
- 25 Bentz, B. Z., Chavan, A. V., Lin, D., Tsai, E. H. R., Webb, K. J. Fabrication and application of heterogeneous printed mouse phantoms for whole animal optical imaging. *Applied Optics*. **55** (2), 280-287, doi:10.1364/AO.55.000280, (2016).
- 26 Diep, P. *et al.* Three-dimensional printed optical phantoms with customized absorption and scattering properties. *Biomedical Optics Express*. **6** (11), 4212-4220, doi:10.1364/BOE.6.004212, (2015).
- 27 Pogue, B. W., Patterson, M. S. Review of tissue simulating phantoms for optical spectroscopy, imaging and dosimetry. *Journal of Biomedical Optics*. **11** (4), 041102-

- 041102-041116, doi:10.1117/1.2335429, (2006).
- 28 de Bruin, D. M. *et al.* Optical phantoms of varying geometry based on thin building blocks with controlled optical properties. *Journal of Biomedical Optics*. **15** (2), 025001-025001-025010, doi:10.1117/1.3369003, (2010).
- 29 Boyle, A. J. *et al.* In vitro performance of a shape memory polymer foam-coated coil embolization device. *Medical Engineering & Physics*. (2017).
- 30 Hwang, W., Singhal, P., Miller, M. W., Maitland, D. J. In Vitro Study of Transcatheter Delivery of a Shape Memory Polymer Foam Embolic Device for Treating Cerebral Aneurysms. *Journal of Medical Devices*. **7** (2), 020932-020932-020932, doi:10.1115/1.4024338, (2013).

2. P. 8, line 270. A prior paper has demonstrated that micro-CT is a useful approach for evaluating phantom morphology (Wang et al., Opt Lett 2014), however, is there any evidence for recommending high resolution MRI or implying that it is as effective as micro-CT for assessing phantom geometry? A suitable, fact-based statement regarding geometric verification should be provided.

**Additional information on the capabilities of micro-CT and high-resolution MRI have been added with corresponding references (page 8, lines 320-323). To improve this section, a micro-CT was taken of the healthy lung tissue phantom for verification of the internal structure.**

3. It is unclear why the statement regarding use of animals was provided on p. 8, line 282, as while the work seems to have been inspired by animal studies, no actual measurements of animal tissues are described in the methods or results section. If this refers to optical property measurements, then the methods for performing tissue measurements should be described.

**This is meant to refer to the measurements of tissue optical properties. The same system and software was used to determine tissue optical properties as phantom optical properties. A statement of this has been added to the manuscript on page 8, lines 338-339.**

4. Is there a reason why the absorption coefficient chosen for inflamed tissue was 30% lower than the mean biological value?

**Table 5 has been edited to include the new values for the recipes from another reviewer's comment. Also, the inflamed mouse tissue optical properties have been updated to only include samples from mice that had been infected with  $10^6$  bacteria, rather than a range of infectious doses, which may cause variable amounts of inflammation. 3 additional lung samples were excluded due to a high standard deviation within the absorption at the wavelength of interest.**

5. Figure 3 is not sufficiently described in the main text; the only description is provided in the figure caption, which is not sufficient. A thorough description of what was imaged and its meaning should be provided in the text.

**A description of the phantoms and imaging methods has been added to the manuscript on page 8, lines 357-362.**

6. The manuscript provides only cursory evaluation of the fabricated morphology. To adequately validate the proposed approach, a more thorough and quantitative assessment of build quality - i.e., how the final structure compares to the original specified geometry - should be provided.

**A micro CT of the completed phantom has been placed as the new panel B in the figure (now Figure 7). A verification of the internal geometry can be found in table 6.**

7. Methods for performing the final validation imaging are not sufficiently described. What systems and optical parameters were used? How was "internal illumination" performed?

**A detailed description of the imaging system has been added to page 9, lines 379-385.**

8. Figure 4 is not sufficiently described in the text. What are the dimensions of this phantom? How much of the phantom region contains channels? However, it's not clear what this result proves, as it seems likely the same findings would have been achieved by changing the absorption coefficient in a phantom without channels.

**This figure is meant to show that the effects of optical properties are conserved with the internal structure. There should be a difference in surface irradiance with and without the internal structure. This figure is meant to show phantoms of different optical properties with internal illumination, provided by the internal void. The phantoms imaged in this figure are 1.8 cm x 2 cm in the image, and are 1.1 cm thick. A scale bar has been added to Figure 4 to show this scale, and a statement to clarify the purpose of the figure has been added to the manuscript on page 9, lines 387-389.**

9. Information on the stability of the phantoms over a period of weeks to months would be useful as well.

**No photo-fading or degradation of optical properties on that time scale is expected. To address this comment, we measured the samples from the phantoms produced 2 years ago. A degradation of the scattering coefficient was found, and that information has been added to table 5. References for the stability of the phantoms in shorter terms have been added to the manuscript (page 10 lines 428-432).**

#### **New references:**

- 27 Pogue, B. W., Patterson, M. S. Review of tissue simulating phantoms for optical spectroscopy, imaging and dosimetry. *Journal of Biomedical Optics*. **11** (4), 041102-041102-041116, doi:10.1117/1.2335429, (2006).
- 28 de Bruin, D. M. *et al.* Optical phantoms of varying geometry based on thin building blocks with controlled optical properties. *Journal of Biomedical Optics*. **15** (2), 025001-025001-025010, doi:10.1117/1.3369003, (2010).

#### **Reviewer #2:**

##### **Manuscript Summary:**

This manuscript discusses a protocol for creating optical phantoms with complex designs that mimic the optical properties of tissue. The method is illustrated for a murine airway designed as a void. The motivation for the tissue-mimicking phantoms is adequate and compelling. The authors provide look-up tables for material recipes to mimic the absorption and scattering properties of tissue in PDMS.

##### **Major Concerns:**

Obtaining the correct optical properties is highly dependent on the correct choice of scattering (TiO<sub>2</sub>) and absorptive (India ink) material amounts. The tables provided give a range of values, but only arbitrary values are filled in. Moreover, within a given table, there is no clear trend in the values that

makes it possible or reasonable to interpolate the missing values, and this lack of a clear trend is not explained (and would be more obvious if the values were given in graphical, rather than tabular, format). The tables are unique for each wavelength, and it is also assumed that the parameters for a non-specified wavelength can be determined by interpolation, which seems an impossible task given the current format and lack of trend in the data as described just now.

**In general, the recipes should have low concentrations of both particles at the upper left corner, and high concentrations of both in the lower right. While the tables from the first submission follows that general trend, the data for these look-up tables has been re-evaluated. Any recipes that only had one sample measured were discarded from the tables. Outliers were also discarded for the recipes that were kept. New samples were also made and included with the average of the old samples for these recipes, and agreed well. In addition, surface plots for the absorption and scattering coefficients of these recipes have been added to the figure list to show the general trend. We believe the lookup tables do still provide useful information, as the recipes for a desired absorption coefficient and scattering coefficient may not match up between the two surface plots. More description about what to expect by changing concentrations of optical particles has been added to the manuscript (page 10, lines 423-428).**

The goal is to be able to mimic complex tissue structures. However, the current protocol only enables one to do this in shape, but does not give a clear methodology for how to do this in terms of multiple tissue types or properties, either in a layered format or other, more complex geometry. The structure of lung tissue is not homogeneous, but this method seems to only clearly apply to homogeneous phantoms.

**In general, yes, this limits the outer mold to one homogenous material. However, the void which remains after dissolving the 3D printed part can be filled with a polymer mixture with other optical properties. Also, a phantom is not limited to the number of dissolvable parts within a single mold. If desired, ten printed parts could be molded into the phantom and dissolved, and each material void could be filled with an optically unique material. This information has been added to the introduction of the manuscript (page 3, lines 123-128).**

Minor Concerns:

The method is assumed to be very generalizable, but there are clear limitations that are not stated. For example, the recipes for absorption and scattering coefficients are appropriate for PDMS, but may not be appropriate if another material is used.

**This is true. A statement regarding the material-specific nature of these recipes has been added to the manuscript on page 4, line, 141.**

The design of the phantom creates a void, which may be useful to measure reflectance, but this design is not suitable for transmission measurements, as the bulk material thickness is not controlled (only the internal void shape is controlled). In particular, it is not clear how this protocol could be applied to a structure that is not a void.

**Phantoms fabricated with this method would be best suited for diffuse reflectance methods.**

**However, we do use them for imaging with internal illumination and external detection (figure 7), which is a transmission measurement. In addressing an earlier comment, we discussed applying this**

**method to a phantom that would consist of multiple materials, rather than one material and a void (see response to Major concern #2).**

The visible improvement in Fig 1b over 1a is marred by the fuzziness of the picture. In fact, there are some structures that appear to be residual air bubbles that suggest the method for degassing may not work as well as described. Labels in the figure that clarify what appear to be imperfections in Fig 1b would be appreciated.


**The panels with this photo in figure 1 and figure 6b (previously figure 3b) have been updated with a clearer white-light photo of the polished, degassed phantom.**

The geometry of the image in Fig 4 is totally unclear. Is this a top-down image? What are we seeing and what do the counts represent?

**A computer simulation and micro-CT of the phantom have been added to the figure (now Figure 7) as panels A and B. The language in the caption has also been changed to reflect that the orientation of the phantom is the same as figure 6 (previously figure 3).**

The results in Table 5 are somewhat unconvincing. The absorption coefficient of healthy tissue is close to that of the phantom, but that of the inflamed tissue seems far off (and is JUST out of the range of one standard deviation). Similarly for the reduced scattering coefficient, although both values are within the tolerable target range, the coefficient for the healthy phantom seems much more similar to what is expected for inflamed tissue, and the values for the healthy and inflamed phantoms are both much more similar to each other than are the healthy and inflamed tissue.

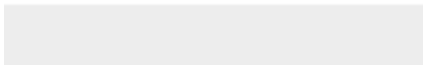
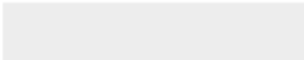
**Table 5 has been edited to include the new values for the recipes addressed in your second comment. Also, the inflamed mouse tissue optical properties have been updated to only include samples from mice that had been infected with  $10^6$  bacteria, rather than a range of infectious doses, which may cause variable amounts of inflammation. 3 additional lung samples were excluded due to a high standard deviation within the absorption at the wavelength of interest.**



[Click here to access/download](#)  
**Supplemental Coding Files**  
test.rxt



Click here to access/download  
**Supplemental Coding Files**  
4gen\_50 percent.stl

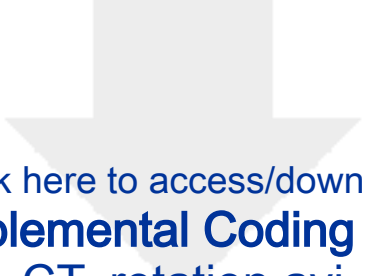




Click here to access/download  
**Supplemental Coding Files**  
phantom CT\_flythru.avi







Click here to access/download  
**Supplemental Coding Files**  
CT\_rotation.avi

